Rodlike Counterions near Charged Cylinders: Counterion Condensation and Intercylinder Interaction

Minryeong Cha,[1,*] Sunghan Ro,[2,*] and Yong Woon Kim[1,2,†]
[1]Graduate School of Nanoscience and Technology, Korea Advanced Institute of Science and Technology, Deajeon 34141, Korea
[2]Department of Physics, Korea Advanced Institute of Science and Technology, Deajeon 34141, Korea

(Received 4 January 2018; revised manuscript received 15 March 2018; published 30 July 2018)

We study a system composed of like-charged cylinders and dumbbell-like counterions, with the focus laid on the role of the internal structure of counterions, using Monte Carlo simulations. The dumbbell ions are found to exhibit novel counterion condensation behavior governed by their length. Effective electrostatic interactions mediated between charged parallel cylinders also turn out significantly different from the case of pointlike ions, as a result of the complex interplay between the spatially separated charge distribution in the dumbbell counterions, their orientation, and the curvature of the charged cylinder. We show that at a weak-to-moderate electrostatic coupling strength, where effective like-charge interactions are usually found to be repulsive, the intercylinder interaction can become attractive and display a distinctive sensitivity to the cylinder curvature and dumbbell size, proving the significant effect of ion structure.

DOI: 10.1103/PhysRevLett.121.058001

Rigid charged biopolymers such as DNA, microtubules, and actins are involved in various biological functions and are usually modeled by charged cylinders. One of the most striking features of these systems in the presence of multivalent counterions is the like-charge attraction [1–6], which contradicts the prediction of the mean-field Poisson-Boltzmann (PB) theory. In recent years, the PB theory has been improved to include, e.g., ionic correlations and fluctuations [7–10], a finite volume of ions [11,12], and even a nonuniform dielectric constant of the solvent medium [13,14]. Most studies have assumed counterions as pointlike particles without internal structures.

Some multivalent ions, however, have extended rodlike structure with well-separated charge distributions along the backbone. Typical examples are stiff polyamines such as spermine and spermidine [15,16]. For these ions, the validity of the point-particle assumption becomes questionable, and, moreover, they are effective condensation agents to induce bundle formations or collapses of various charged biopolymers [15–19]. Recently, there have been several theoretical attempts to take into account the internal structure of counterions [20–27]. They found that two like-charged *planar* surfaces attract each other in the presence of rodlike counterions, perhaps surprisingly, even in the mean-field regime where pointlike counterions lead only to repulsion [21–23] (for recent reviews, see, e.g., Refs. [25,26], and references therein).

Then a question arises: Does the attraction between two like-charged planar surfaces mediated by the rodlike counterions persist even for cylindrical surfaces? Notwithstanding the fact that, on most relevant length scales, charged biopolymers can be regarded as cylinders [28–31], this critical question has not been addressed, and the answer is not straightforward, because the two geometries are fundamentally different in several aspects. Furthermore, the electrostatic interactions are governed by counterions around charged surfaces, and the two geometries have distinct counterion condensation behaviors even for pointlike ions. In the case of a cylinder, as electrostatic potential competes with confinement entropy, a characteristic condensation transition, referred to as the Manning transition, occurs at a critical temperature [32–39]; i.e., not all pointlike counterions are bound to the cylindrical surface. In contrast, for a charged plane, electrostatic energy dominates entropy to condense all pointlike counterions to the surface. How the counterion condensation is altered for structured ions is also an interesting question by itself. In a nutshell, taking the rodlike structure of counterions into consideration, the condensation behavior of counterions and the effective interactions mediated by them in cylindrical geometry come as unanswered questions.

In this Letter, via Monte Carlo (MC) simulations, we address these problems and present a systematic study on charged cylinders in the presence of rodlike counterions, modeled as dumbbells. We find that the dumbbell structure of counterions leads to a characteristic condensation behavior that depends on the dumbbell size. Moreover, the dumbbell size and cylinder curvature drastically affect the intercylinder interaction at a weak-to-moderate coupling strength. We provide direct evidence that ionic structure and charged surface curvature interplay in a complex way resulting in unique equilibrium phases that cannot be extrapolated from the case of pointlike ions or planar geometry.

System.—We first study the counterion condensation by considering a system composed of a charged cylinder and N dumbbell-like counterions [Fig. 1(a)]. The cylinder of

 © 2018 American Physical Society

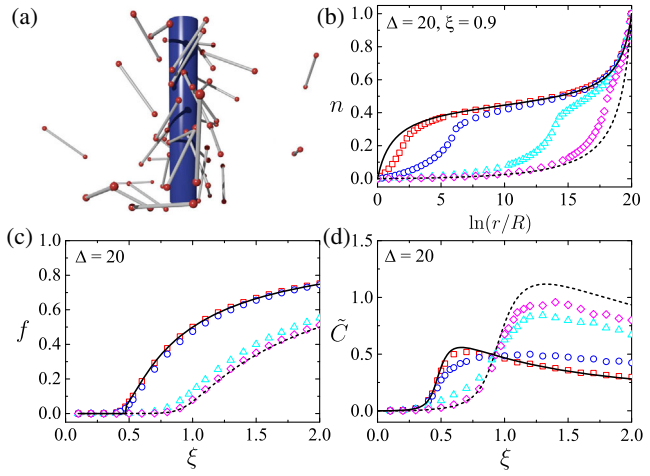

FIG. 1. (a) Snapshot of a charged cylinder (blue) and dumbbell-like counterions where two q-valent pointlike charges (red) are connected by a thin rod (gray) [$\Xi = 0.1$, $\xi = 1$, $d = 4$]. (b) Cumulative density profiles, (c) condensed counterion fraction, and (d) heat capacity in the weak-coupling regime ($\Xi = 0.1$) for $\Delta = 20$, where various dumbbell sizes are examined, such as $\alpha \equiv (\ln d)/\Delta = 0.1$ (squares), 0.3 (circles), 0.7 (triangles), and 0.9 (diamonds) [40]. Solid (dotted) lines represent the PB predictions for $2q$ (q)-valent pointlike charges.

radius R is at the origin and has a uniform surface charge distribution: $\sigma(\mathbf{r}) = \sigma_s \delta(r - R)$. A dumbbell ion consists of two q-valent pointlike charges connected by a thin rod of length d, and the number density of ions is $\rho(\mathbf{r}) = \sum_{j=1}^{N} [\delta(\mathbf{r} - \mathbf{r}_j) + \delta(\mathbf{r} - \mathbf{r}_j - \mathbf{d}_j)]$, where $\mathbf{d}_j = d\hat{\mathbf{n}}_j$ with $\hat{\mathbf{n}}_j$ being a unit vector along the jth dumbbell orientation. The canonical partition function is given as

$$\mathcal{Z}_N = \frac{1}{N!} \prod_{j=1}^{N} \int d\mathbf{r}_j d\hat{\mathbf{n}}_j \Omega(\mathbf{r}_j, \mathbf{r}_j + \mathbf{d}_j) \exp[-\beta(\mathcal{H} - \Sigma_s)],$$

where the Hamiltonian in units of $k_B T = \beta^{-1}$ reads as $\beta\mathcal{H} = (\ell_B/2) \int d\mathbf{r} d\mathbf{r}' Q(\mathbf{r}) v(\mathbf{r}, \mathbf{r}') Q(\mathbf{r}')$ with $v(\mathbf{r}, \mathbf{r}') = 1/|\mathbf{r} - \mathbf{r}'|$ and $Q(\mathbf{r}) = q\rho(\mathbf{r}) - \sigma(\mathbf{r})$, and Σ_s indicates all the self-energy terms of $v(\mathbf{r}, \mathbf{r})$. Here, $\ell_B \equiv e^2/(4\pi\varepsilon\varepsilon_0 k_B T)$ is the Bjerrum length in a medium of dielectric constant ε. The factor $\Omega(\mathbf{r}, \mathbf{r}')$ takes account of the excluded-volume effect of a dumbbell ion with a cylinder; it is zero if a dumbbell overlaps with the cylinder and unity otherwise. We assume the dumbbells as lines with no thickness and thus ignore steric interaction between them. We introduce the electrostatic coupling parameter measuring the strength of ionic correlations as $\Xi = 2\pi q^3 \ell_B^2 \sigma_s$ [7–9], and the Manning parameter indicating the strength of counterion-cylinder attraction as $\xi = q\ell_B \tau$ with line charge density $\tau = 2\pi R \sigma_s$. We rescale all lengths by the Gouy-Chapman length $\mu = 1/(2\pi q \ell_B \sigma_s)$ as $\tilde{\mathbf{r}} = \mathbf{r}/\mu$, but, for simplicity of notation, the tilde on rescaled lengths shall be dropped hereafter.

To minimize finite-size effects in simulations, we impose periodic boundary conditions along the cylinder axis (the z axis), and the Coulomb interactions between periodic images of the central box of height H are counted through the rapidly converging Lekner-Sperb resummation [9,35,36]. We assume that the system is confined inside an outer cylindrical boundary of radius L, or $\Delta = \ln(L/R)$ in the logarithmic scale. For an efficient sampling of the phase space, not only centrifugal sampling by transforming the radial coordinate to the logarithmic scale [35,36] but also a direct exchange move between condensed and decondensed counterions are used [37–39].

Counterion condensation.—In Fig. 1(b), we present simulation results for the cumulative counterion density, $n(r) = (1/\xi) \int_R^r dr' r' \langle \rho(r') \rangle / (2\pi \ell_B \sigma_s^2)$ with $\rho(r)$ being the radial distribution of counterions, where the bracket $\langle \cdots \rangle$ denotes the thermal average with Boltzmann weight. The results are presented as a function of the logarithmic radial distance, $y = \ln(r/R)$, for dumbbell ions of different sizes at the weak-coupling (WC) regime. For comparison, we provide the PB predictions for pointlike counterions at a given Δ. The solid line is for N pointlike counterions with valency $2q$, and the dotted line is for $2N$ pointlike counterions with valency q, satisfying the charge neutrality in either case. In Fig. 1(b), $n(r)$ of dumbbell ions is observed to follow either the $2q$ behavior (solid line) or the q behavior (dotted line) according to the radial distance r and dumbbell size d. At a distance r, much larger than the dumbbell size ($r \gg d$), the data points obey the $2q$ behavior, but at shorter distances ($r \ll d$), they agree well with the q behavior. The relatively sharp crossover between the two behaviors occurs around the dumbbell size $r \sim d$; see, e.g., for $\alpha \equiv (\ln d)/\Delta = 0.7$, the crossover occurs at $\ln(r/R) \approx 14$.

The counterion condensation is characterized by a fraction of counterions that remain within a finite distance from the cylinder. For pointlike ions, the condensed fraction f is defined by using the inflection-point criterion [41,42]. In the case of dumbbell ions, there exists an ambiguity in adopting the inflection-point criterion [43], but we compute the condensed fraction f as $n(y_*)$ with $y_* = \ln(r_*/R) = \Delta/2$, which reasonably quantifies the condensed fraction in consistency with the behaviors of the heat capacity. In Fig. 1(c), we present f as a function of the Manning parameter ξ. For large dumbbell ions with $\alpha > 1/2$, the condensed fraction f is well described by the q-valent pointlike behavior (dotted line), leading to the condensation transition at $\xi \approx 1$. In contrast, small dumbbell ions with $\alpha < 1/2$ start to condense at $\xi \approx 1/2$, and f complies with the $2q$-valent behavior (solid line). Such two distinguishing features of dumbbell ions according to their lengths are also evidenced in the dimensionless heat capacity per particle [35,36], $\tilde{C} = \langle (\beta\mathcal{H} - \langle \beta\mathcal{H} \rangle)^2 \rangle / (N\Delta)$, presented in Fig. 1(d). We also examined the strong-coupling (SC) regime and found the

same behavior; i.e., two different condensation points are observed at $\xi = 1/2$ or 1, depending on d [44]. The critical behavior of condensation emergent only in the limit of $\Delta \to \infty$ (for pointlike ions, see Refs. [35–38]) is not our concern.

Intercylinder interactions.—We now turn to the interaction of two like-charged cylinders mediated by dumbbell-like counterions. We consider two identical cylinders of radius R and surface charge density σ_s, parallelly aligned along the z axis with an axial separation of D. We calculate the intercylinder forces by employing two independent methods, i.e., using the free energy estimated through the Jarzynski equality [45,46] and the direct force evaluation within MC simulations as detailed in Ref. [31]. In the first method, two cylinders thermalized at a fixed initial distance are pulled apart to a certain distance D along a specified protocol. Repeating the protocol, we measure the work w expended at each pulling to give the free energy difference between the initial and final distances as $\langle e^{-\beta w}\rangle_w = e^{-\beta \mathcal{F}(D)}$, where $\langle\cdots\rangle_w$ denotes the average with respect to the work distribution [45,46].

In Figs. 2(a) and 2(b), we show the rescaled forces per unit length, $\tilde{F} = 2\pi\beta\Xi(F/H)$, for various d and ξ as a function of D at the WC limit ($\Xi = 0.1$); $F = -\partial\mathcal{F}/\partial D$ with $\mathcal{F}$ obtained via the Jarzynski equality (lines) and direct force evaluation (symbols). According to the PB theory for pointlike ions, two like-charged objects always repel. In the case of dumbbell ions, our results show otherwise. Even at weak coupling, for d (or ξ) greater than a certain value,

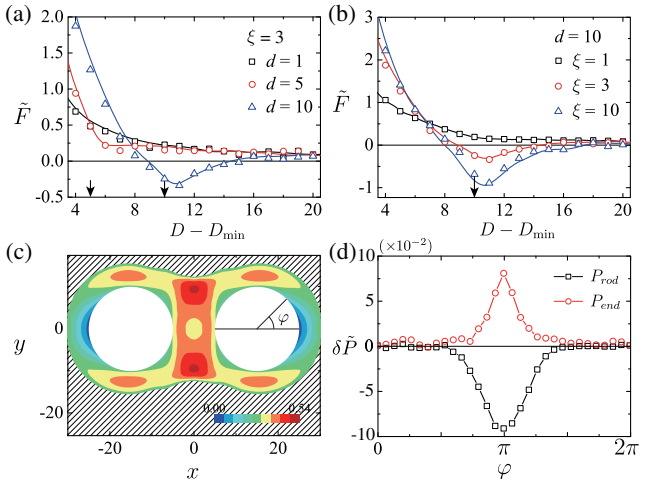

FIG. 2. Rescaled forces $\tilde{F}$ at the WC regime ($\Xi = 0.1$) versus $D - D_{\min}$ with $D_{\min} = 2R$ for various (a) d and (b) ξ. Two independent methods are employed: Jarzynski equality (solid lines) and direct force evaluation (symbols). $D - D_{\min} = d$ is indicated as an arrow. (c) Contour plot of the orientational order parameter of dumbbells when $D - D_{\min} = d + 1 = 11$ and $\xi = 10$. (d) Osmotic pressure profiles, along the cylinder surface due to rods and end points of the dumbbells, relative to a reference value: $\delta\tilde{P}(\varphi) \equiv \tilde{P}(\varphi) - \tilde{P}(0)$, where $\tilde{P} = 2\pi\beta\Xi\xi P$. The same parameters as in (c) are used.

cylinders attract each other (indicated by negative $\tilde{F}$) around a region of $D - 2R \sim d$; see the results for $d = 10$ in Fig. 2(a) and for $\xi = 3$, 10 in Fig. 2(b). For $\Xi \ll 1$, through the saddle-point approximation of the grand-canonical partition function [23], we can derive the extended PB equation for dumbbell ions as $\nabla^2\phi(\mathbf{r}) = -4\Lambda\int d\hat{\mathbf{n}}\Omega_2(\mathbf{r}, \mathbf{r}+\mathbf{d})e^{-\beta\phi(\mathbf{r})-\beta\phi(\mathbf{r}+\mathbf{d})}$, where ϕ is the electrostatic potential, Λ is rescaled fugacity, and Ω_2 represents the steric constraint of dumbbells with the two cylinders. For a quantitative understanding, one has to solve the PB equation, a highly nonlinear integrodifferential equation, under complicated geometrical constraints specified by Ω_2, which is a formidable task. Yet, looking at the orientational configuration of dumbbell ions, we can intuitively understand these attractions. Figure 2(c) presents the averaged orientational order parameter along the x axis, $\chi = \langle(\sin\theta\cos\varphi)^2\rangle$, with θ (φ) being the polar (azimuth) angle between the dumbbell orientation and the z (x) axis, and $\chi = 1/3$ for random orientations. On the exterior side, the dumbbell ions close to cylinders tend to be parallelly aligned along the cylinder axis (as denoted by small χ), while in the intervening region between the two cylinders, a finite portion of dumbbell ions tend to be perpendicularly oriented, leading to larger χ.

These perpendicularly oriented dumbbell ions are essential to induce the intercylinder attraction by means of two distinct effects: (i) energetic bridging and (ii) reducing osmotic pressure in the intervening region. Effect (i) results from a tendency for two end point charges in a perpendicularly aligned dumbbell to sit simultaneously near the charged surfaces where the potential energy minima are located. This mechanism also exists for the attraction between planar surfaces, as detailed in Refs. [21–23]. What is unique for curved surfaces is effect (ii): When perpendicularly aligned, we have less collision between a cylinder and a rod connecting two end points in a dumbbell [gray rod in Fig. 1(a)]. In consequence, the osmotic pressure in between the cylinders is reduced, pushing the two cylinders toward each other. In Fig. 2(d), we show the osmotic pressure profiles due to end points ($P_{\rm end}$) and rods ($P_{\rm rod}$) of dumbbells along the cylinder surface, where the angle φ is defined as in Fig. 2(c). The pressure is given by the normal component of the osmotic force per unit height on the infinitesimal line segment $Rd\varphi$ as $dF_n^{\rm osm}(\varphi)/H = -P(\varphi)Rd\varphi$. Contrary to the planar surface, the pressure profiles are inhomogeneous along the cylinder surface. $P_{\rm rod}$ is reduced in the intervening space (around $\varphi = \pi$), which dominates over the enhancement of $P_{\rm end}$ and results in the net attraction. This demonstrates the significant contributions of the rod-cylinder collisions due to the finite cylinder curvature.

Now we consider the interactions at the SC regime. As exemplified in Figs. 3(a) and 3(b) showing the rescaled force $\tilde{F}$ at $\Xi = 10^4$, we find the attraction occurs only for $\xi > 1/3$ (see data for $\xi = 0.5$, 0.8 in comparison with

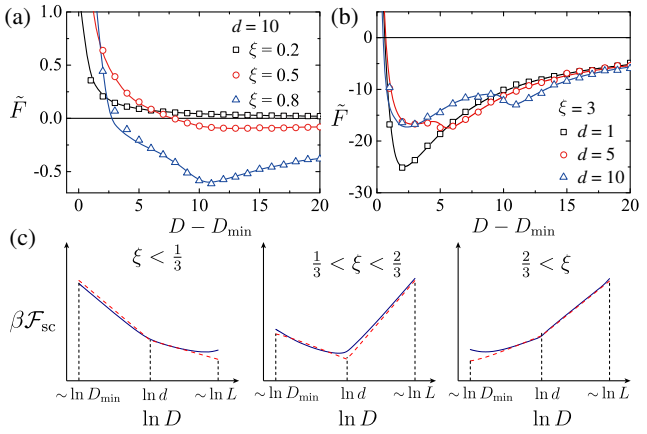

FIG. 3. Rescaled forces $\tilde{F}$ at the SC regime ($\Xi = 10^4$) versus $D - D_{\min}$ for various (a) ξ and (b) d. Symbols are MC simulation results, and lines are calculated from the SC free energy [Eq. (1)] showing perfect agreement. (c) Comparison of the asymptotic expressions (dashed lines) Eqs. (2) and (3), with a numerical evaluation of Eq. (1) (solid lines). From left to right, $\xi = 0.3$, 0.6, 0.8 at $d = 10^3$ and $L = 10^6$.

$\xi = 0.2$). The interaxial distance at which the force vanishes corresponds to the equilibrium distance $D_{\rm eq}$ that differs depending on ξ: For $1/3 < \xi < 2/3$, $D_{\rm eq} \sim d + 2R$, and for $\xi > 2/3$, $D_{\rm eq} \sim 2R$, indicating that two cylinders are almost in contact to form a compact bound state. In order to understand these results quantitatively, we extend the SC theory for pointlike ions to the case of dumbbell ions as below.

For $\Xi \gg 1$, through the virial expansion of the grand-canonical partition function and the Legendre transformation, the canonical SC free energy $\mathcal{F}_{\rm SC}$ is written as [29,30]

$$\beta\mathcal{F}_{\rm SC} = U_0 - N \ln I, \tag{1}$$

where $U_0 = -2N\xi \ln D$ is the electrostatic repulsion between bare cylinders and the single-particle partition function is $I = \int d^2r \int d\hat{\mathbf{n}}\Omega_2(\mathbf{r}, \mathbf{r}') \prod_{i=1}^{2} e^{-u(r_i)-u(r_i')}$ with $u(r) = 2\xi \ln r$. The radial distances of two end points of a dumbbell from the ith cylinder are denoted by r_i and r_i', respectively. A numerical evaluation of $\mathcal{F}_{\rm SC}$ shows perfect agreement with simulation results; compare the force evaluated using Eq. (1) (lines) and simulation data (symbols) in Figs. 3(a) and 3(b). Furthermore, the D dependence of $\mathcal{F}_{\rm SC}$ can be found by the asymptotic analysis of scaling behaviors of I [29,30,44]: When $\xi < 1/2$, the asymptotic expressions of the SC free energy per particle read as (apart from a D-independent constant)

$$\frac{\beta\mathcal{F}_{\rm SC}}{N} \sim \begin{cases} -2\xi \ln D & \text{for } D \ll d, \\ -2(1-3\xi) \ln D & \text{for } D \gg d. \end{cases} \tag{2}$$

If $\xi > 1/3$, a minimum is developed in the free energy around $D \sim d$. Otherwise, the free energy is a monotonically decreasing function of D, and the force always becomes repulsive [Fig. 3(c)]. On the other hand, when $\xi > 1/2$, we obtain

$$\frac{\beta\mathcal{F}_{\rm SC}}{N} \sim \begin{cases} -2(2-3\xi) \ln D & \text{for } D \ll d, \\ 2\xi \ln D & \text{for } D \gg d. \end{cases} \tag{3}$$

If $\xi > 2/3$, the free energy monotonically increases with D, leading to close contact of cylinders. In Fig. 3(c), we compare these asymptotic expressions with the full numerical evaluations of Eq. (1). Both are in excellent agreement with each other, and their dependence on ξ and D explains well the behaviors presented in Figs. 3(a) and 3(b). We also note that, for $D \ll d$, $\mathcal{F}_{\rm SC}$ follows the expression of pointlike ions in Refs. [29,30], while, for $D \gg d$, $\mathcal{F}_{\rm SC}$ agrees with the pointlike result with replacing q with $2q$. At the SC regime, dumbbells in the intervening space show a short-ranged liquidlike positional order along the cylinder axis, and orientationally they are aligned along the x axis at $D_{\rm eq} \sim d + 2R$ while along the z axis at $D_{\rm eq} \sim 2R$.

Phase diagram.—So far, we have considered the limiting values of the coupling strength, i.e., $\Xi \to 0$ (WC) or $\Xi \to \infty$ (SC), but, for most of the practical applications, the regime of an intermediate Ξ has no less importance. In Fig. 4, we present the phase diagram, indicating the repulsion and attraction regions in the parameter space for various Ξ; i.e., on the right sides of phase boundaries denoted by lines, the attraction occurs at corresponding Ξ. The parameter space is spanned by the Manning parameter (or, equivalently, rescaled cylinder radius $R = \xi$) and the rescaled dumbbell size. At $\Xi = 10^4$, the phase boundary agrees with the SC theory prediction; cylinders attract each other, irrespective of d, only if $\xi > 1/3$. At $\Xi = 0.01$, on the other hand, the attraction occurs when $d > d_*$, the critical dumbbell size d_* is a function of the Manning parameter, and, at $\xi \to \infty$ (corresponding to the planar limit), we find $d_* \approx 4$, consistent with the results for

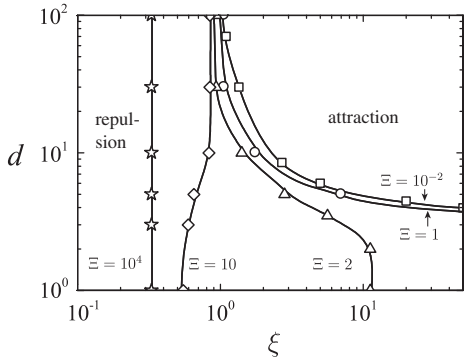

FIG. 4. Phase diagram of intercylinder interactions for various Ξ, obtained from MC simulations. Attraction occurs at ξ and d lying on the right side of the line given for a specified Ξ. The lines for $\Xi = 10^{-2}$ and $\Xi = 10^4$ are converged results to the WC limit ($\Xi \to 0$) and the SC limit ($\Xi \to \infty$), respectively.

charged plates [23]. At a weak-to-moderate coupling strength, the phase boundaries show a very sensitive dependence on the dumbbell size as well as the cylinder curvature (compare the phase boundaries for $\Xi = 1$, 2, and 10). Considering spermidines as rodlike ions, biopolymers such as actin, microtubules, and the M13 virus have parameter values in the range of $\Xi = 2$–20, $\xi = 5$–30, and $d = 2$–6, which roughly corresponds to the region showing the sensitive dependence on d and ξ [47]. Our result suggests that the rodlike structures of counterions could be critical to understanding the correct phase behaviors of rigid polyelectrolytes in the presence of polyamine ions, especially at a low coupling strength relevant to physiological conditions.

This research was supported by a National Research Foundation of Korea (NRF) grant funded by the Korean government (Grant No. NRF-2017R1A2B4007608).

*These authors contributed equally.
†Corresponding author.
y.w.kim@kaist.ac.kr

[1] V. A. Bloomfield, Biopolymers **31**, 1471 (1991).
[2] N. Grønbech-Jensen, R. J. Mashl, R. F. Bruinsma, and W. M. Gelbart, Phys. Rev. Lett. **78**, 2477 (1997).
[3] R. Podgornik, D. Rau, and V. A. Parsegian, Biophys. J. **66**, 962 (1994).
[4] B.-Y. Ha and A. J. Liu, Phys. Rev. Lett. **79**, 1289 (1997).
[5] T. E. Angelini, H. Liang, W. Wriggers, and G. C. L. Wong, Proc. Natl. Acad. Sci. U.S.A. **100**, 8634 (2003).
[6] H. Boroudjerdi, Y. W. Kim, A. Naji, R. R. Netz, X. Schlagberger, and A. Serr, Phys. Rep. **416**, 129 (2005).
[7] R. R. Netz and H. Orland, Eur. Phys. J. E **1**, 203 (2000).
[8] R. R. Netz, Eur. Phys. J. E **5**, 557 (2001).
[9] A. G. Moreira and R. R. Netz, Phys. Rev. Lett. **87**, 078301 (2001).
[10] Y. Burak and H. Orland, Phys. Rev. E **73**, 010501(R) (2006).
[11] I. Borukhov, D. Andelman, and H. Orland, Phys. Rev. Lett. **79**, 435 (1997).
[12] I. Borukhov, J. Polym. Sci. B **42**, 3598 (2004).
[13] A. Abrashkin, D. Andelman, and H. Orland, Phys. Rev. Lett. **99**, 077801 (2007).
[14] A. Levy, D. Andelman, and H. Orland, Phys. Rev. Lett. **108**, 227801 (2012).
[15] L. C. Gosule and J. A. Schellman, Nature (London) **259**, 333 (1976).
[16] D. J. Needleman, M. A. Ojeda-Lopez, U. Raviv, H. P. Miller, L. Wilson, and C. R. Safinya, Proc. Natl. Acad. Sci. U.S.A. **101**, 16099 (2004).
[17] J. Pelta, F. Livolant, and J.-L. Sikorav, J. Biol. Chem. **271**, 5656 (1996).
[18] E. Raspaud, M. O. de la Cruz, J.-L. Sikorav, and F. Livolant, Biophys. J. **74**, 381 (1998).
[19] J. C. Butler, T. Angelini, J. X. Tang, and G. C. L. Wong, Phys. Rev. Lett. **91**, 028301 (2003).
[20] J. DeRouchey, R. R. Netz, and J. O. Rädler, Eur. Phys. J. E **16**, 17 (2005).
[21] K. Bohinc, A. Iglič, and S. May, Europhys. Lett. **68**, 494 (2004).
[22] S. May, A. Iglič, J. Reščič, S. Maset, and K. Bohinc, J. Phys. Chem. B **112**, 1685 (2008).
[23] Y. W. Kim, J. Yi, and P. A. Pincus, Phys. Rev. Lett. **101**, 208305 (2008).
[24] M. Kanduč, A. Naji, Y. S. Jho, P. A. Pincus, and R. Podgornik, J. Phys. Condens. Matter **21**, 424103 (2009).
[25] A. Naji, M. Kanduč, J. Forsman, and R. Podgornik, J. Chem. Phys. **139**, 150901 (2013).
[26] *Electrostatics of Soft and Disordered Matter*, edited by D. Dean, J. Dobnikar, A. Naji, and R. Podgornik (Pan Stanford, Singapore, 2014).
[27] S. Dutta and Y. S. Jho, Phys. Rev. E **93**, 012504 (2016).
[28] D. Andelman, in *Soft Condensed Matter Physics in Molecular and Cell Biology*, edited by W. C. K. Poon and D. Andelman (Taylor & Francis, New York, 2006).
[29] A. Naji and R. R. Netz, Eur. Phys. J. E **13**, 43 (2004).
[30] A. Naji, A. Arnold, C. Holm, and R. R. Netz, Europhys. Lett. **67**, 130 (2004).
[31] M. Kanduč, A. Naji, and R. Podgornik, J. Chem. Phys. **132**, 224703 (2010).
[32] R. M. Fuoss, A. Katchalsky, and S. Lifson, Proc. Natl. Acad. Sci. U.S.A. **37**, 579 (1951).
[33] G. S. Manning, J. Chem. Phys. **51**, 924 (1969).
[34] F. Oosawa, *Polyelectrolytes* (Marcel Dekker, New York, 1971).
[35] A. Naji and R. R. Netz, Phys. Rev. Lett. **95**, 185703 (2005).
[36] A. Naji and R. R. Netz, Phys. Rev. E **73**, 056105 (2006).
[37] M. Cha, J. Yi, and Y. W. Kim, Sci. Rep. **7**, 10551 (2017).
[38] M. Cha, J. Yi, and Y. W. Kim, Eur. Phys. J. E **40**, 70 (2017).
[39] J. P. Mallarino, G. Téllez, and E. Trizac, J. Phys. Chem. B **117**, 12702 (2013).
[40] The dumbbell size reads as $d/R = e^{\alpha\Delta}/\xi$ in units of R, and the q-valent condensation can occur at a much-reduced d (of the order of nanometers) as considering smaller Δ.
[41] M. Deserno, C. Holm, and S. May, Macromolecules **33**, 199 (2000).
[42] B. O'Shaughnessy and Q. Yang, Phys. Rev. Lett. **94**, 048302 (2005).
[43] For dumbbells, when $\xi > 1/2$, $n(y)$ has two local minima in its first derivative, which makes the choice of the inflection point less obvious. However, using $y_* = \Delta/2$ gives a reasonable approximation of a condensed fraction, which will be discussed in detail elsewhere.
[44] S. Ro, M. Cha, J. Yi, and Y. W. Kim (unpublished).
[45] C. Jarzynski, Phys. Rev. Lett. **78**, 2690 (1997).
[46] G. E. Crooks, J. Stat. Phys. **90**, 1481 (1998).
[47] We model a polyamine as a dumbbell with each end point having half of the total charges of polyamine.